Cement and Concrete Research 100 (2017) 176–185

Contents lists available at ScienceDirect

Cement and Concrete Research

journal homepage: www.elsevier.com/locate/cemconres

Solution chemistry of cubic and orthorhombic tricalcium aluminate hydration

Rupert J. Myers[a,b,*], Guoqing Geng[a], Erich D. Rodriguez[c,d], Priscila da Rosa[c], Ana Paula Kirchheim[c], Paulo J.M. Monteiro[a]

[a] Department of Civil and Environmental Engineering, University of California, Berkeley, CA, United States
[b] Yale School of Forestry & Environmental Studies, Yale University, New Haven, CT, United States
[c] Department of Civil Engineering, Universidade Federal do Rio Grande do Sul (UFRGS), Porto Alegre, RS, Brazil
[d] Department of Civil Engineering, IMED, Passo Fundo, RS, Brazil

ARTICLE INFO

Keywords:
Kinetics
Hydration
Retardation
$Ca_3Al_2O_6$
Sulfate
Cement

ABSTRACT

This paper presents a solution chemistry-focused analysis of orthorhombic and cubic tricalcium aluminate (orth-C_3A and cub-C_3A, respectively) hydration. It is shown that the different solubilities of cub- and orth-C_3A influence the bulk aqueous Ca to Al concentration ratio and the C_3A/solution interface chemistry. The results are consistent with the bulk solution chemistry controlling orth-C_3A dissolution, and with cub-C_3A dissolution controlled by the formation of an Al-rich leached layer and adsorption of Ca-sulfur ion pair complexes onto this layer. The polynaphthalene sulfonate-based admixture used here is identified to modify the solution chemistry and retard cub-C_3A dissolution. Strategies to inhibit C_3A dissolution in Portland cement are discussed.

1. Introduction

The setting time and workability of Portland cement (PC) concrete critically depend on the kinetics of tricalcium aluminate (C_3A) hydration. The rapid dissolution of C_3A in water and initial precipitation of solid hydration products, including 'Al_2O_3-Fe_2O_3-mono' (AFm) phases (e.g., OH-AFm, C_4AH_x, where the water content, x, is a function of the relative humidity and is typically 13 or 19 [1], or $C_2AH_{7.5}$ [2]), and the subsequent formation of katoite (C_3AH_6) [2–4], can cause fresh PC concrete to prematurely and irreversibly lose fluidity and workability ('flash set'), resulting in poor strength development [5]. For these reasons, a small amount (typically 2–5 wt%) of solid calcium sulfate is added to PC to retard C_3A dissolution. Gypsum ($C\bar{S}H_2$) is most commonly added, although hemihydrate ($C\bar{S}H_{0.5}$) and anhydrite ($C\bar{S}$) are also used and/or may be produced by dehydration of gypsum during cement production.

The C_3A phase occurs as a series of solid solutions in PC, typically involving substitutions of Ca for 2 M ($M_{2x}Ca_{3-x}Al_2O_6$), where M is an alkali metal, normally Na or K. The Na and K present in PC clinker (~1 wt% Na_2O + K_2O [5,6]) are mainly distributed into soluble solid sulfates and C_3A, with partitioning of K biased towards incorporation in arcanite [6–9]. The structure of C_3A is cubic (cub-C_3A) at low Na content ($0 \le x \le 0.10$) and orthorhombic (orth-C_3A) at moderate Na content ($0.16 \le x \le 0.20$) [5,10–12], with a miscibility gap existing over intermediate compositions ($0.10 \le x \le 0.16$) [5,10–12]. The alkali content in PC is typically too low to produce monoclinic C_3A ($0.20 \le x \le 0.25$) [5–7,13,14]. The crystal structures and composition limits of the Na- and K-substituted C_3A solid solutions are similar [12]. Other substitutions can occur e.g., Mg for Ca, and Si or Fe for Al, but the crystal symmetry of this phase is reportedly only affected by the alkali content [11]. The extent that cub-C_3A dissolution is inhibited by calcium sulfate is directly related to the amount added [15,16]. However, orth-C_3A dissolution occurs more rapidly in aqueous sulfate solutions than in water, and orth-C_3A also dissolves faster than cub-C_3A in aqueous sulfate solutions [17–20], meaning that the crystal chemistry of C_3A and the calcium sulfate content are both important factors in PC hydration, as well as in the production of high performance PC concrete.

The reactions involved in cub-C_3A-water-calcium sulfate and PC systems at bulk $\bar{S}/A$ molar ratios of ~0.05 [15] and ~0.25 [8], respectively, are mechanistically comparable. In these systems, ettringite ($C_6A\bar{S}_3H_{32}$) precipitates from relatively sulfur- and Ca-rich aqueous solutions ($10 < [S] < 20$ mmol L^{-1} and $20 < [Ca] < 40$ mml L^{-1}) [15,21] and is the major solid hydration product before complete gypsum dissolution [8]. Ettringite is typically also the major solid phase produced by orth-C_3A hydration in the presence of calcium sulfate in

* Corresponding author.
E-mail addresses: rupert.myers@gmail.com (R.J. Myers), guoqinggeng1989@gmail.com (G. Geng), erich.rodriguez@imed.edu.br (E.D. Rodriguez), priscila.rosa@ufrgs.br (P. da Rosa), anapaula.k@ufrgs.br (A.P. Kirchheim), monteiro@berkeley.edu (P.J.M. Monteiro).

http://dx.doi.org/10.1016/j.cemconres.2017.06.008
Received 8 February 2017; Received in revised form 20 June 2017; Accepted 29 June 2017

this range of bulk $\bar{S}$/A concentration ratios [18]. Hexagonal platelets (most likely AFm-type phases) are initially formed on hydrating orth- [17] and cub-C_3A [15,21,22] particles, and a surface layer of solid reaction products with ill-defined morphology is identified when viewed on the micron length scale during this initial reaction period (up to a maximum of a few hours) [17,23]. The chemistry of this layer has been described in terms of AFm-type phases in the cub-C_3A-gypsum-water system [24]. X-ray diffraction (XRD) and calorimetry data for this system [25] suggest that an initially formed amorphous aluminate phase (possibly this ill-defined layer of solid reaction products) destabilises over time, leading to ettringite precipitation.

Ettringite precipitation continues in cub-C_3A systems with bulk molar $\bar{S}$/A ratios $< \sim 0.25$ until the calcium sulfate source has completely reacted, which is reported to coincide with renewed rapid dissolution of cub-C_3A, a release of heat, precipitation of $\bar{S}$-AFm ($C_4A\bar{S}H_{12}$, where the water content is again a function of the relative humidity [1]), and destabilisation of the initially formed ettringite [15,16]. Reduced aqueous Ca and sulfur concentrations are also measured in calcium sulfate containing aqueous cub-C_3A systems after complete dissolution of the calcium sulfate source [15,21,26]. Less information is reported for orth-C_3A hydration relative to cub-C_3A hydration, although ettringite is the dominant solid phase produced from orth-C_3A and gypsum hydration after 14 days at a bulk molar $\bar{S}$/A ratio of 0.75 [18].

Consensus is only now being reached on the rate controlling factors of cub- and orth-C_3A dissolution in the presence of calcium sulfate, despite decades of research on this topic [4,9,15,16,18,21,26–33]. It is increasingly thought that a dissolution rate controlling 'barrier' covering cub-C_3A particles (e.g., [9,19,34]) does not exist in the gypsum-containing aqueous cub-C_3A system throughout the induction period [35]. This argument is supported by micro- and macro-scale analyses and a crystallographic understanding of the chemical system [15]. As a result, and consistent with research published decades earlier [29,30,33], numerous researchers have hypothesised that adsorption of sulfur and/or Ca complexes is the key cub-C_3A dissolution rate controlling factor in aqueous calcium sulfate solutions [20,21,24,35,36]. However, these hypotheses are not all supported by the geochemical literature, which report little or no adsorption of SO_4^{2-} and SeO_4^{2-} onto Al and Fe (hydr)oxides above pH 7–10 [37–40] (these complexes exhibit similar adsorption behaviour). Recent zeta potential, Ca and sulfur *K*-edge X-ray absorption spectroscopy (XAS) results similarly confer a lack of evidence for specific adsorption of SO_4^{2-} complexes onto partially dissolved cub-C_3A particles in aqueous solutions [41]. A more complex role of adsorption phenomena in inhibiting cub-C_3A dissolution was thus proposed for better consistency with the relevant literature [41]. It attributes the adsorption of Ca-sulfur ion pair complexes onto partially dissolved cub-C_3A particles, the surfaces of which are relatively Al-rich, to increase the local saturation extent near C_3A surface sites and consequently retard the cub-C_3A dissolution rate.

Polynaphthalene sulfonate (PNS) is a synthetic commercial water-reducing admixture that is commonly added to PC concrete in addition to calcium sulfate to further modify its workability. It is typically polydispersed with a mean molecular mass of $\gg$1000 Da [20,42], and contains $-SO_3^-$ ligands [43]. It is reported to adsorb onto hydrated PC particles and retard C_3A dissolution [20,41,44], although its effect on the solution chemistry of C_3A hydration systems is poorly understood. Much less information has also been published on the rate-controlling factor(s) of orth-C_3A dissolution in aqueous solutions relative to cub-C_3A hydration systems, although existing research suggests that the solution chemistry plays a key role [9,17,20,45].

Here, inductively coupled plasma optical emission spectroscopy (ICP-OES) and pH experiments are performed and supplemented by thermodynamic modelling to better understand the role of the solution chemistry on C_3A hydration in three systems: (1) in water; (2) in water and with gypsum; and (3) in aqueous solutions containing PNS and with gypsum. It has been demonstrated that the transition between inhibited and rapid dissolution of cub-C_3A in aqueous calcium sulfate containing solutions is strongly linked to the solution chemistry, although only a few publications have reported aqueous phase chemical composition data [15,21,26,33]. Solution chemistry datasets for orth-C_3A systems are scarcer [45]. This work is also needed to provide a more coherent description of the dissolution inhibiting role that adsorption phenomena plays in retarding cub-C_3A dissolution in calcium sulfate containing aqueous systems, particularly in light of recent results [41]. Complementary isothermal calorimetry (IC), XRD, and thermogravimetric analysis (TGA) data are obtained and used to complete the analysis. The results are discussed to provide an advanced description of cub- and orth-C_3A dissolution in alkaline Ca- and sulfur-rich aqueous solutions, i.e., in a similar chemical environment to that which exists in fresh PC concrete.

2. Materials and methods

2.1. Materials for ICP-OES, pH and XRD

The cub-C_3A (cub-C_3A_1, $Na_{0.06}Ca_{3.11}Al_2O_{6.14}$, Mineral Research Processing Cie, hereafter MRP) and orth-C_3A (orth-C_3A_2, $Na_{0.37}Ca_{2.92}Al_2O_{6.11}$, MRP) powders used to produce the hydrated samples measured by ICP-OES, pH, and XRD were synthesised by firing $CaCO_{3\ (s)}$, $Al_2O_{3\ (s)}$, and $Na_2CO_{3\ (s)}$ (all from Merck) twice at 1350 °C for 2 h in platinum vessels. The material was ground to a fine powder in an intermediate grinding step.

The chemical composition, purity and crystal structures of cub-C_3A_1, orth-C_3A_2, and the gypsum precursors used, gypsum_1 (Fisher Scientific) and gypsum_2 (Sigma-Aldrich) (the use of two gypsum precursors is discussed below), were quantified by X-ray fluorescence (XRF), TGA, XRD, and Rietveld analysis (estimated uncertainty = ± 3 wt%). The data show that cub-C_3A_1 contains 95 wt% cub-C_3A (Powder Diffraction File (PDF)# 01-070-0839), 4 wt% katoite (C_3AH_6, PDF# 00-024-0217), and 1 wt% portlandite (CH, PDF# 01-072-0156). Orth-C_3A_2 was identified to contain ~89 wt% orth-C_3A (PDF# 01-070-0859), ~10 wt% cub-C_3A, and ≤1 wt% CH. Gypsum_1 is pure, and gypsum_2 contain 93 wt% gypsum (PDF# 01-070-0982) and 7 wt% hemihydrate (PDF# 01-081-1848). Free lime (CaO) was not identified in any of the X-ray diffractograms of the cub- and orth-C_3A powders used. Thermogravimetric analysis (TGA) confirmed the presence of CH and additionally showed that small amounts of $Al(OH)_3$ (½AH_3) had formed in both cub-C_3A_1 and orth-C_3A_2 prior to sample preparation (< 2.5% mass lost to 550 °C). Therefore, these results indicate that the cub-C_3A_1 and orth-C_3A_2 powders used were slightly hydrated during storage and/or sample preparation.

The Brunauer-Emmett-Teller (BET) surface areas of cub-C_3A_1 (523 $m^2\,kg^{-1}$, d_{50} = 16.8 μm), orth-C_3A_2 (762 $m^2\,kg^{-1}$, d_{50} = 9.2 μm), gypsum_1 (474 $m^2\,kg^{-1}$, d_{50} = 415 μm), and gypsum_2 (313 $m^2\,kg^{-1}$, d_{50} = 54.3 μm) were measured on a Quantachrome Nova 1000 after heating to 300 °C under vacuum for 4 h for cub- and orth-C_3A, and at 70 °C under vacuum for 10 min for gypsum. Particle size distributions were measured on a Cilas Granulometer 1180 in isopropyl alcohol after ultrasonication at 38 kHz for 60 s. Additional experimental details and results are reported in Appendix A (Electronic Supporting Information, ESI).

2.2. Materials for IC

Hydrated samples analysed by IC were synthesised using orth-C_3A_2, gypsum_2 and a different batch of cub-C_3A (cub-C_3A_2) to the powder used in the ICP-OES, pH and XRD experiments (cub-C_3A_1), but synthesised using the same method. This cub-C_3A_2 powder was characterised using the same instruments as the solid precursors described in Section 2.1. It was determined to contain ≥ 99 wt% cub-C_3A by XRD and Rietveld analysis, to have a d_{50} of 20.8 μm (Appendix A, ESI), and a BET surface area of 473 $m^2\,kg^{-1}$, i.e., cub-C_3A_2 is slightly coarser and

purer than cub-C_3A_1. The materials described in Section 2.1 were chosen for consistency with those used in recent synchrotron-based research [41,46], while cub-C_3A_2 was selected for consistency with work performed at Universidade Federal do Rio Grande do Sul. The significance of using two different batches of cub-C_3A is discussed further in the analysis of the results.

2.3. Sample preparation

Polymer-free samples were prepared at a liquid/solid mass ratio (l/s) = 10, which was chosen to provide enough solution to analyse the samples by ICP-OES at low solids mass and excess water needed for full hydration. Deionised water was used in samples measured by IC. High purity water (18.2×10^6 Ω cm, produced using a Barnstead NANOpure II with a filter size = 0.2 μm) was otherwise used. Gypsum was mixed with cub- or orth-C_3A prior to the addition of water at a mass ratio of 1.0 C_3A:0.40 gypsum ($\bar{S}$/A molar ratio ≈ 0.15) in the absence of PNS (Mira 151, W. R. Grace & Co.-Conn.). Another set of samples was synthesised by mixing cub-C_3A and gypsum, and then adding these solids to a dilute aqueous PNS solution at a mass ratio of 0.06 PNS: 1 cub-C_3A. The same mass of cub-C_3A and an equivalent bulk sulfur concentration to the PNS-free gypsum containing samples was used. These conditions represent 'adsorption saturation' of PNS in a system containing cub-C_3A reacted with an aqueous K_2SO_4 solution after 30 min [20], and so is an approximation because the extent of PNS adsorption onto C_3A likely changes from one C_3A source to another. The solids fraction and sulfur, Na, Al, and Ca concentrations in the undiluted PNS solution were determined by ASTMC494 to be 54 wt% and by ICP-OES to be 1.5×10^3 mmol L^{-1}, 2.7×10^3 mmol L^{-1}, 8.0 mmol L^{-1}, and 13 mmol L^{-1}, respectively.

Samples analysed by ICP-OES, XRD, TGA, and pH measurements were synthesised and cured in sealed polypropylene vessels under ambient laboratory conditions (24 ± 2 °C), and continuously mixed until filtration. Samples were filtered using 0.45 μm nylon filters. The filtrates were collected and then the solids were immediately washed with acetone, dried under 24 ± 2 °C and 20 kPa for ≥ 5 days, and then stored at 24 ± 2 °C in vacuum-sealed bags until analysis.

2.4. Methods

The materials and corresponding analytical methods used are shown in Table 1.

Filtered solids (hydration stopped by washing with acetone) were analysed by XRD using a PANalytical X'Pert PRO diffractometer with an X'Celerator detector, Co Kα radiation generated at 40 kV and 40 mA, a step size of 0.017° 2θ, and a dwell time of 0.4 s. X-ray diffractograms are reported with respect to the magnitude of the scattering vector $Q = 4\pi\sin(\theta)/\lambda$ ($Å^{-1}$). Supernatant Ca, Al, sulfur, and Na concentrations were determined by ICP-OES on a Perkin Elmer 5300 DV using Ar plasma after dilution by at least a factor of 5 with 2 vol% $HNO_{3\ (aq)}$ (which itself was synthesised by titrating 70 vol% trace metal grade $HNO_{3\ (aq)}$, Sigma-Aldrich, into 18.2×10^6 Ω cm water). A relative uncertainty of ± 10% is estimated and practical minimum detection limits for Ca, Al, sulfur, and Na are 0.01 mmol L^{-1}, 0.003 mmol L^{-1}, 0.03 mmol L^{-1}, and 0.01 mmol L^{-1} in the samples investigated, respectively. Supernatant OH^- concentrations were determined directly after filtration using an Accumet pH meter (Fisher Scientific) that was calibrated against NaOH solutions of known concentrations (estimated absolute uncertainty is ± 0.3 pH units).

An isothermal Tam Air calorimeter (TA Instruments) operated at 25 °C was used to follow the hydration of cub- and orth-C_3A samples (20 μW sensitivity). Thermal equilibrium of the raw materials was achieved by storing them in a desiccator at 25 °C for 30 min prior to measurement. The calorimeter temperature was also maintained at 25 °C prior to measurement. Baseline stabilisation was established prior to introducing vials into the calorimeter. Samples were prepared by mixing 0.5–1.0 g of solids (gypsum, cub-C_3A, orth-C_3A), deionised water, and PNS at the same proportions previously specified (Section 2.3) for 2 min in a calorimetry vial by hand before being introduced into the calorimeter. The decision to hand mix samples for 2 min was made using preliminary tests, which showed that this condition yielded homogenized samples and highly reproducible results. Heat flows were measured for 48 h after the vials were introduced into the calorimeter. The IC data obtained are normalised to the total masses of solids added.

Effective saturation indices (SI^{eff}) for relevant solid phases in the C-A-$\bar{S}$-H system were calculated using measured supernatant Ca, Al, and sulfur concentrations, and Eq. (1):

$$SI_i^{eff} = \frac{1}{n_i}\log_{10}\left(\frac{IAP_i}{K_{s0,i}}\right) \quad (1)$$

where IAP_i is the ion activity product of the i^{th} solid phase, $K_{s0,i}$ is the solubility product of the i^{th} solid phase, and n_i is the total stoichiometric number of ions in the dissolution reaction defined for the i^{th} solid phase (Table C3 in Appendix C, ESI). Supernatants with positive values of SI^{eff} are supersaturated, are undersaturated at negative SI^{eff} values, and are saturated at $SI^{eff} = 0$ with respect to the simulated solid phases. If the measured Ca, Al, and sulfur concentrations in the supernatants were below the detection limit, concentrations of 0.01 mmol L^{-1}, 0.003 mmol L^{-1}, 0.03 mmol L^{-1} were used in Eq. (1), respectively. Activity coefficients for charged aquo species were calculated using the Gibbs free energy minimisation GEM-Selektor v.3 software (http://gems.web.psi.ch/) [47,48] and the Truesdell-Jones form of the extended Debye-Hückel equation with ion size and extended term parameter for KOH ($\dot{a}$ = 3.67 Å and b_γ = 0.123 kg/mol) [49]. The activity of water was determined using the osmotic coefficient and $b_\gamma I$ was used to determine activity coefficients for neutral aqueous species, where I is the ionic strength. The CEMDATA14.01 thermodynamic database was used (Appendix C, ESI) [8,50–61].

Table 1
Materials and corresponding analytical methods used here.

Materials	Methods
Cub-C_3A_1, water	ICP-OES, pH, XRD, TGA[a], thermodynamic modelling
Cub-C_3A_1, gypsum_1, water	ICP-OES, pH, XRD, thermodynamic modelling
Cub-C_3A_1, gypsum_1, PNS, water	ICP-OES, pH, XRD
Cub-C_3A_2, water	IC
Cub-C_3A_2, gypsum_1, water	IC
Cub-C_3A_2, gypsum_1, PNS, water	IC
Cub-C_3A_2, gypsum_2, water	IC
Cub-C_3A_2, gypsum_2, PNS, water	IC
Orth-C_3A_2, water	ICP-OES, pH, XRD, IC, TGA[†], thermodynamic modelling
Orth-C_3A_2, gypsum_2, water	ICP-OES, pH, XRD, IC, TGA[†], thermodynamic modelling

[a] Supporting TGA measurements are shown in Appendix B (ESI).

3. Results and discussion

3.1. Hydration of orth- and cub-C_3A in water

Dissolution of orth-C_3A in water is incomplete after 2896 min (~48 h) (Fig. 1). Orth-C_3A is expected to remain strongly undersaturated as it dissolves in water (Fig. 1B), although the SI^{eff} of cub-C_3A (used as a proxy for orth-C_3A here) is lower at > 601 min (~10 h) relative to earlier hydration times. Katoite forms immediately after dissolution begins, out-competing the other 'near-saturated' phases (i.e., phases with $SI^{eff} \approx 0$), which are CH and $C_2AH_{7.5}$ here (Fig. 1B–C).

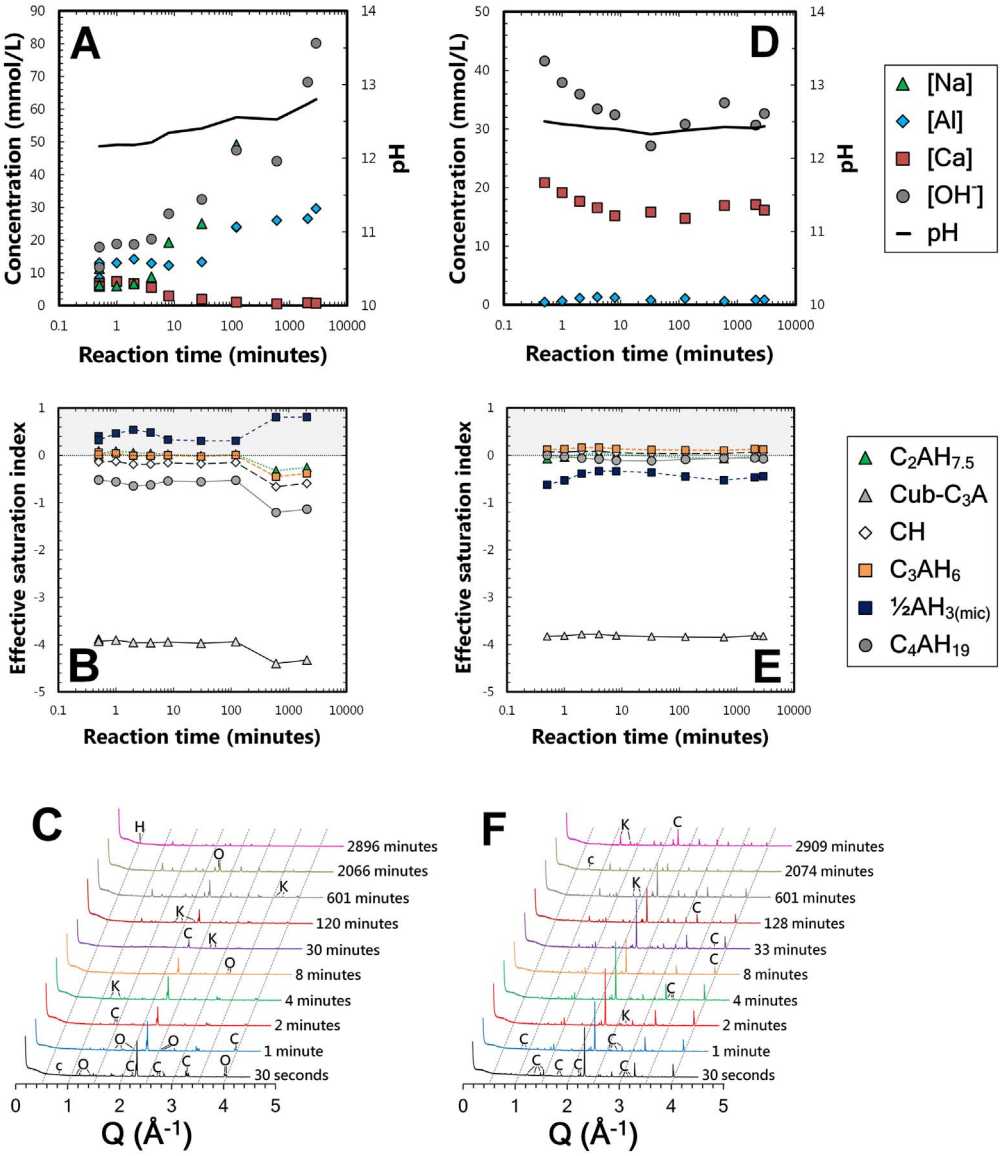

Fig. 1. Results from ICP-OES, pH and XRD analysis of (A–C) orth-C_3A_2 and (D–F) cub-C_3A_1 hydrated in water. The phase identification labels in the diffractograms are O = orth-C_3A, C = cub-C_3A, K = katoite, H = C_4AH_{19}-like OH-AFm and c = $C_4A\overline{C}H_{11}$. The grey and white regions in (B) and (E) represent supersaturation ($SI^{eff} > 0$) and undersaturation ($SI^{eff} < 0$) of solid phases with respect to the aqueous phase, respectively. The dashed and solid lines in (B–C) and (E–F) are eye guides only. Microcrystalline is abbreviated as mic.

Microcrystalline $\frac{1}{2}AH_3$ is supersaturated in this system but undetected by XRD, although additional TGA data confirm the presence of $\frac{1}{2}AH_3$ at 4 min of hydration (Appendix B, ESI). OH-AFm (C_4AH_{19}-like, PDF# 00-042-0487) is identified by XRD after both 2066 and 2896 min (~34 and ~48 h) of hydration despite being significantly undersaturated at these times. Small amounts of $C_4A\overline{C}H_{11}$ (PDF# 01-087-0493) are detected in some samples, which is caused by superficial carbonation during sample storage, preparation, and analysis.

In general, the concentrations of aqueous Al, Na, and OH^- increase and the Ca concentration decreases with increasing orth-C_3A dissolution extent (Fig. 1A), such that the aqueous molar Ca/Al ratio ($Ca/Al_{[aq]}$) decreases from 0.56 at 1 min to 0.02–0.04 between 120 and 2896 min (2 and ~48 h) of hydration (Fig. 2). This deficiency of Ca in the aqueous phase relative to bulk orth-C_3A and katoite (i.e., $Ca/Al_{[aq]} \ll 1.5$), and the initial lack of solid hydration products with Ca/Al molar ratios > 1.5, indicates that the $Al_6O_{18}^{18-}$ ring structures dissolve preferentially to the Ca structures in orth-C_3A and suggests that a relative excess of Ca exists at the solid/solution interface of partially dissolved orth-C_3A particles in water (a schematic of the C_3A/solution interface is shown in [41]). These results and this interpretation are consistent with work conducted by Glasser and Marinho [45], who predicted the surface of partially hydrated orth-C_3A particles (dissolving in water) to

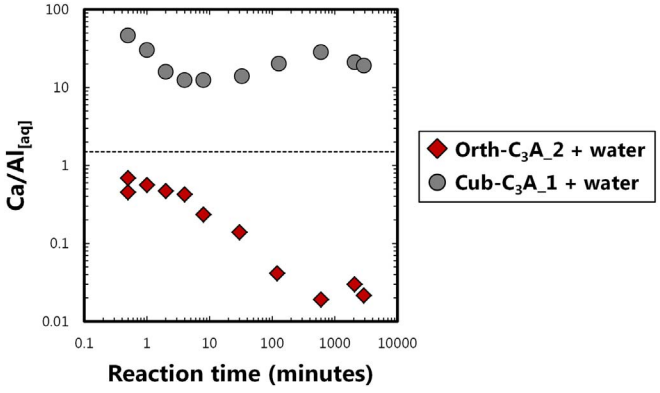

Fig. 2. $Ca/Al_{[aq]}$ values of supernatants collected from samples containing orth-C_3A_2 (red diamonds) or cub-C_3A_1 (grey circles) hydrated in water (estimated uncertainty = 10%). The dashed black horizontal line represents the ideal molar Ca/Al ratio in C_3A (1.5). (For interpretation of the references to colour in this figure legend, the reader is referred to the web version of this article.)

become progressively more deficient in Al at lower l/s values than used in their experiments (l/s ≈ 360). The significant reduction in the Ca/$Al_{[aq]}$ to ~2 orders of magnitude less than the initially measured values at > 120 min is somewhat consistent with the identification of OH-AFm (bulk Ca/Al = 2) after 2066 min (~34 h) of hydration (Fig. 1C). Therefore, OH-AFm precipitates as a kinetic product in this orth-C_3A system (as it is strongly undersaturated) when a sufficiently high excess of dissolved Al is present in the aqueous solution.

The IC results for orth- and cub-C_3A hydration in water only show initial heat flow peaks (Fig. 3), which are predominantly related to katoite precipitation (Fig. 1C and F). The maxima of both peaks occurs at ~5 min of hydration. However, the maximum heat flow is greater and more heat is cumulatively released in the cub-C_3A system relative to the orth-C_3A system at 2880 min (48 h), and at this time the cumulative heat release profiles for these systems approach asymptotic and accelerating trends, respectively. This latter difference may be explained by OH-AFm precipitation from orth-C_3A dissolution in water at hydration times > 600 min (Fig. 1C), because this phase is not identified in the XRD results shown here for cub-C_3A hydration in water (Fig. 1F). The faster heat release rate in the cub-C_3A system relative to the orth-C_3A system is consistent with previously reported IC results and a faster hydration rate of cub-C_3A in water [19,20,62].

Dissolution of cub-C_3A in water is also incomplete after 2909 min (~48 h) of hydration (Fig. 1F), consistent with existing results [3,19]. The IC results (Fig. 3) also agree closely with the literature [31] as it shows a single initial heat release peak associated with katoite precipitation, which is the main solid hydration product in this system. The calculated SI^{eff} values show that katoite remains consistently slightly supersaturated up to ~2880 min (~48 h) of hydration (Fig. 1E), demonstrating its high stability in this system. Katoite outcompetes the other 'near-saturated' phases, which are CH, $C_2AH_{7.5}$, C_4AH_{19}, and ½AH_3, to preferentially precipitate. The relatively high stabilities of $C_2AH_{7.5}$ and C_4AH_{19} are consistent with the occasional identification of OH-AFm in hydrated cub-C_3A systems [3,4]. However, these phases are not identified here, which may be caused by superficial carbonation of the samples to destabilise the originally precipitated OH-AFm phases to $C_4A\overline{C}H_{11}$. These results are similar to those obtained for orth-C_3A hydrated in water (Fig. 1A–C), except that the SI^{eff} values calculated for ½AH_3 and C_4AH_{19} are significantly lower and higher, respectively, for cub-C_3A hydrated in water. This difference is caused by the much lower dissolved Al concentration in the cub-C_3A system (Fig. 1A and D).

Dissolution of cub-C_3A is incongruent in water, with dissolution of Ca occurring much faster than Al (Fig. 1D). This result indicates that the Ca structures are more soluble than the $Al_6O_{18}^{18-}$ rings in this phase, such that the initial $Ca/Al_{[aq]}$ = 46 (Fig. 2). The measured concentration of aqueous Al remains ≤ 1.33 mmol L^{-1} here, which is consistently at least an order of magnitude lower than the measured dissolved Ca concentration. This relative deficiency of aqueous Al relative to aqueous Ca, and the predominant precipitation of katoite (Ca/Al = 1.5) in this system (Fig. 1F), indicates that the cub-C_3A/solution interface is relatively enriched in Al and/or a significant amount of Al is incorporated into additional solid hydration products undetected by XRD. The TGA results for this system suggest that ½AH_3 is present at 4 min of hydration (Appendix B, ESI) despite ½AH_3 being undersaturated (Fig. 1E). However, relative enrichment of Al at the partially dissolved cub-C_3A/solution interface in an Al-rich leached layer [63] has been identified by Auger electron spectroscopy in a similar aqueous cub-C_3A system [30], and so is therefore likely to be present in the cub-C_3A sample measured here. It is also possible that this Al-rich layer may contain bound water in chemically similar environments to ½AH_3 and contribute to the mass loss signal in the TGA results. The presence of an Al-rich leached layer in this cub-C_3A system but not in the orth-C_3A and water system is consistent with the reported enhanced solubility of Al in C_3A in more highly concentrated Na-containing aqueous solutions [45]. Recent zeta potential and sulfur and Ca *K*-edge XAS measurements suggest non-specific adsorption of Ca complexes onto the partially hydrated cub-C_3A surface [41], similarly to how Ca complexes onto Al $(OH)_3$ [64], which is also consistent with the presence of an Al-rich leached layer. The relevance of these adsorbed Ca complexes on cub-C_3A hydration is discussed further in Section 3.3.

3.2. Hydration of orth- and cub-C_3A in the presence of gypsum

The addition of gypsum into the orth-C_3A and water system (at a mass ratio of 1.0 C_3A: 0.40 gypsum and bulk molar $\overline{S}/A$ = 0.15) significantly reduces the pH and aqueous Al concentration and increases the dissolved Ca concentration relative to the sulfur-free system before complete gypsum dissolution, which occurs between 8 and 31 min of hydration (Fig. 4A–C). During this period ettringite (PDF# 00-041-1451) is strongly supersaturated and precipitates, outcompeting $C_4A\overline{S}H_{12}$ (PDF# 00-045-0158), which is also supersaturated but to a lesser degree, and the other 'near-saturated' phases (katoite and CH). The remnant orth-C_3A fully dissolves shortly afterwards, between 31 and 123 min of hydration. On complete gypsum dissolution, ettringite becomes undersaturated and is destabilised to $C_4A\overline{S}H_{12}$, although this latter phase also becomes undersaturated, the pH and aqueous Al and Na concentrations increase substantially, and the dissolved Ca and sulfur concentrations are reduced to < 1 mmol L^{-1}. The concentration of aqueous Na is generally similar in the gypsum containing and sulfur-free orth-C_3A systems (Fig. 1A and A). The XRD results for the gypsum containing orth-C_3A system also show that some of these samples were slightly superficially carbonated, as small amounts of $C_4A\overline{C}H_{11}$ precipitates are identified.

This interpretation of orth-C_3A and gypsum hydration in water is supported by the IC results (Fig. 5A). In this system, an early heat flow peak with a maximum at ~4 min of hydration is observed. This peak corresponds to initial orth-C_3A dissolution and principally ettringite precipitation. A secondary heat release peak at ~24 min of hydration is measured, which corresponds to the initial destabilisation of ettringite to $C_4A\overline{S}H_{12}$ on complete gypsum dissolution. A third heat flow peak at

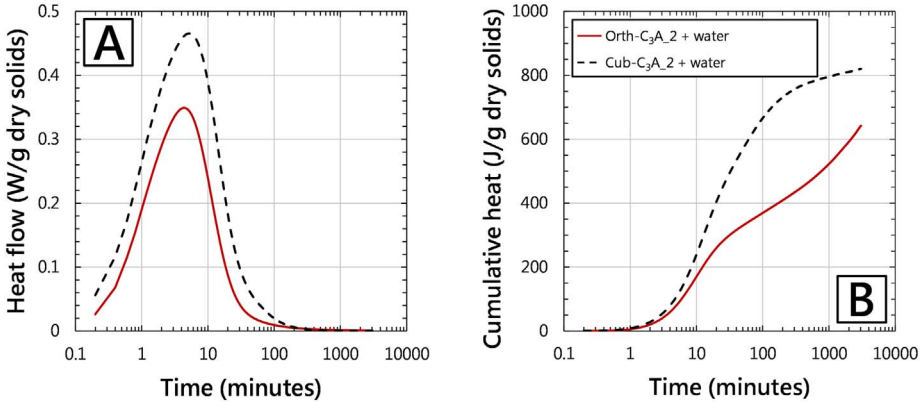

Fig. 3. (A) Heat flow and (B) cumulative heat released from orth-C_3A_2 (solid red lines) and cub-C_3A_2 (dashed black lines) hydrated in water. (For interpretation of the references to colour in this figure legend, the reader is referred to the web version of this article.)

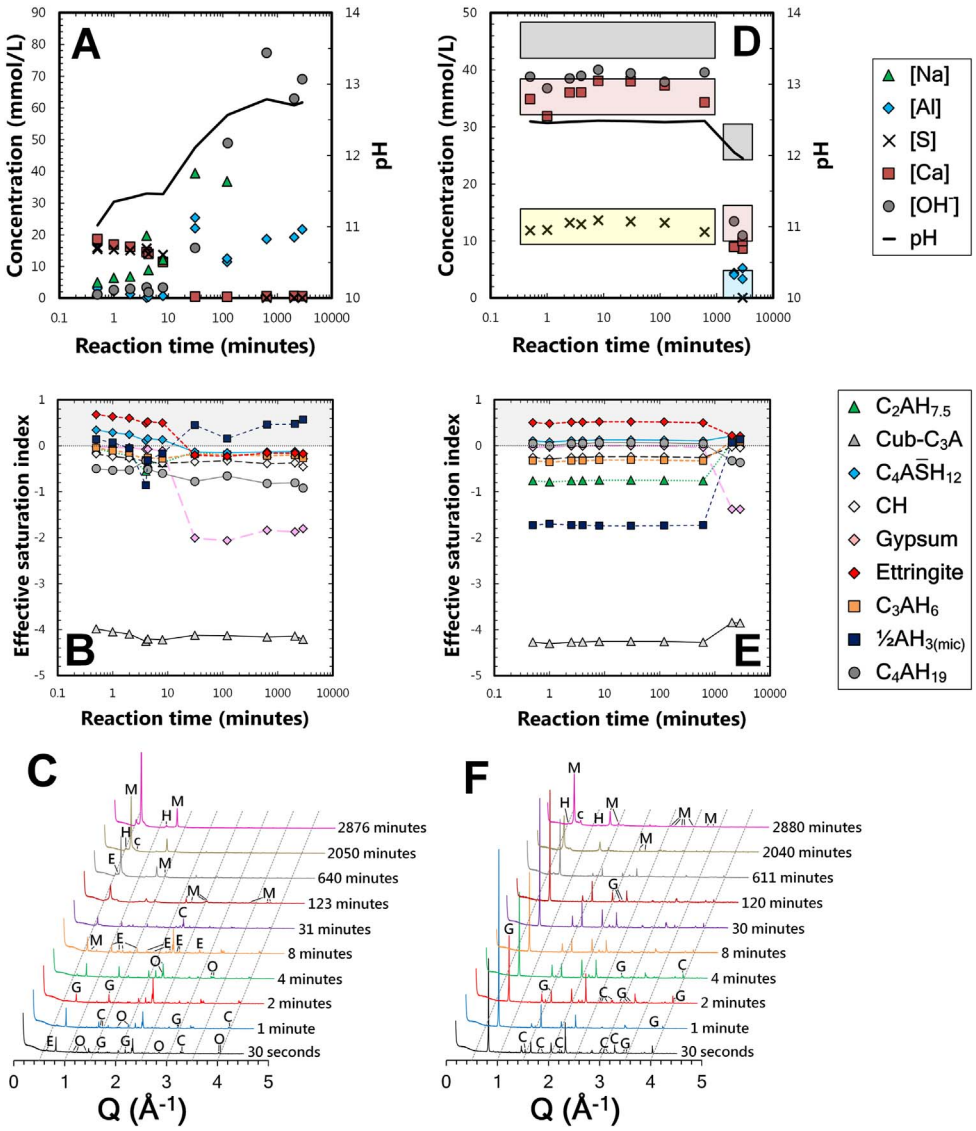

Fig. 4. Results from analysis of (A–C) orth-C_3A_2 and gypsum_2 hydrated in water and (D–F) cub-C_3A_1 and gypsum_1 hydrated in water. The phase identification labels in the diffractograms are C = cub-C_3A, G = gypsum, K = katoite, H = C_4AH_{19}-like OH-AFm, E = $C_6A\bar{S}_3H_{32}$, M = $C_4A\bar{S}H_{12}$ and c = $C_4A\bar{C}H_{11}$. The grey and white regions in (B) and (E) represent super-saturation ($SI^{eff} > 0$) and undersaturation ($SI^{eff} < 0$) of the solid with respect to the aqueous phase, respectively. The red, blue, yellow and grey shaded boxes represent the general range of Ca, Al, S and OH^- concentrations reported in [15] before and after complete gypsum dissolution, overlaid over the respective hydration times measured here, for cub-C_3A and gypsum hydrated in an initially portlandite-saturated aqueous solution. Concentrations of [S] at 30 and 120 min in (A), and [Al] up to 2040 min and [S] at 2040 min in (D), are below the detection limit and so these data points are omitted. The dashed and solid lines in (B–C) and (E–F) are eye guides only. Microcrystalline is abbreviated as mic. (For interpretation of the references to colour in this figure legend, the reader is referred to the web version of this article.)

~210 min (~3.5 h) is also observed, coinciding with the destabilisation of most of the existing ettringite to $C_4A\bar{S}H_{12}$.

The $Ca/Al_{[aq]}$ ratios measured in the gypsum-containing orth-C_3A system ($6 < Ca/Al_{[aq]} < 220$, Fig. 6) are more than an order of magnitude greater than those in the sulfur-free orth-C_3A system during gypsum dissolution (Figs. 1A and 4A), and are also much greater than the bulk molar Ca/Al ratio in orth-C_3A_2 (≈1.5). This relative deficiency of dissolved Al can be explained by its incorporation in ettringite, which precipitates essentially immediately on hydration of orth-C_3A, and also in poorly crystalline ½AH_3, which is 'near-saturated' in this gypsum containing system (Fig. 4B). The assignment of ½AH_3 here is also supported by the TGA results (Appendix B, ESI). The faster dissolution rate of orth-C_3A observed in the presence of gypsum than in water alone [19,20][1] can thus be attributed to the lower aqueous Al concentration in the former system: the addition of gypsum in the orth-C_3A and water system strongly reduces the aqueous Al concentration, consumed through ettringite precipitation. Therefore, the results shown here suggest that the orth-C_3A dissolution rate is controlled by bulk reactive mass transport phenomena in aqueous (gypsum containing) systems.

The addition of gypsum to the cub-C_3A and water system (at a mass ratio of 1.0 C_3A: 0.40 gypsum and bulk molar $\bar{S}/A = 0.15$) significantly increases the aqueous Ca concentration and decreases the dissolved Al concentration ($Ca/Al_{[aq]} > 1000$, Fig. 6), and stabilises the pH at ~12.5 up to between 611 and 2040 min (~10 and 34 h) of hydration (Fig. 4D). Greatly reduced aqueous Ca, sulfur, and OH^- concentrations, and significantly increased aqueous Al concentrations, are measured at later hydration times. These changes coincide with complete gypsum dissolution and: i) the transition to saturation or 'near-saturation' of C_3AH_6, $C_4A\bar{S}H_{12}$, $C_2AH_{7.5}$, ½AH_3, and CH (Fig. 4E); ii) significantly reduced SI^{eff} values for ettringite, C_4AH_{19}, and gypsum (Fig. 4E); and iii) complete dissolution of cub-C_3A (Fig. 4F). Some ettringite also destabilises to OH-AFm after 123 min of hydration despite its undersaturation in this system at these curing times. Therefore, these results are consistent with a rapid destabilisation of ettringite, the predominant solid hydration product in the presence of gypsum and after the initial hydration period [15], to mainly $C_4A\bar{S}H_{12}$ on complete gypsum dissolution at bulk molar $\bar{S}/A$ concentrations < 0.25 [15,16]. Gypsum is consumed at a faster rate in the orth-C_3A system than in this cub-C_3A system, consistent with the lower aqueous Ca concentration in the orth-C_3A system. A similar temporal solid phase assemblage, comparable aqueous Ca, Al, and sulfur concentrations, and slightly higher OH^- concentrations to those measured in this hydrated cub-C_3A and gypsum

[1] Different quantities of C_3A were used in the gypsum-containing and sulfur-free samples analysed here and thus C_3A dissolution rates are not directly comparable between these samples.

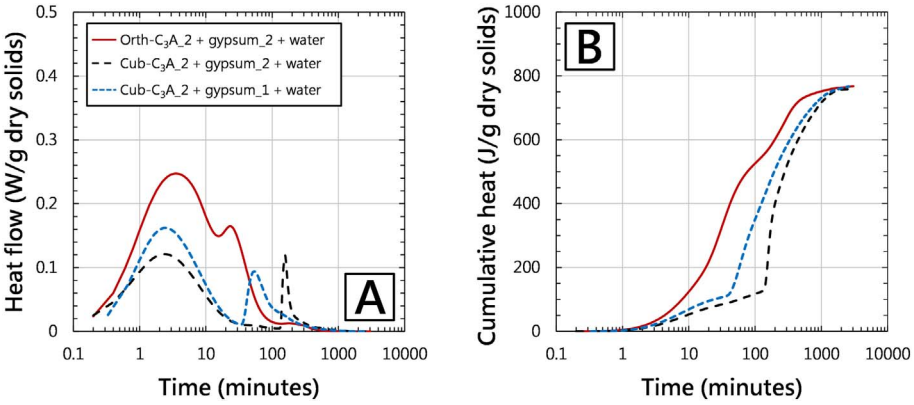

Fig. 5. (A) Heat flow and (B) cumulative heat released from orth-C_3A_2 and gypsum_2 hydrated in water (solid red lines), cub-C_3A_2 and gypsum_2 (dashed black lines) hydrated in water, and cub-C_3A_2 and gypsum_1 (dashed blue lines) hydrated in water. (For interpretation of the references to colour in this figure legend, the reader is referred to the web version of this article.)

system are also reported for cub-C_3A and gypsum hydrated in an initially portlandite-saturated aqueous solution [15] (Fig. 4E, shaded boxes).

The IC results for the gypsum containing cub-C_3A system share the same features present in previously published data (Fig. 5) [15,16,31,34]: i) an early heat release peak with maximum at ~2 min associated with the initial precipitation of solid hydration products; and ii) a sharper secondary heat release peak with maximum at ~60 (gypsum_1) and ~160 min (gypsum_2) depending on the gypsum source. However, the time of these secondary heat release peaks do not match the time that complete consumption of gypsum is identified in the ICP, SI^{eff}, and XRD results reported here, and so this finding contrasts the reported results which link these peaks to the destabilisation of ettringite to $C_4A\bar{S}H_{12}$ and renewed cub-C_3A dissolution. We are unable to explain this discrepancy other than to suggest that it can be attributed to the different durations of mixing employed in the IC (2 min) and ICP-OES, XRD, and TGA (continuously) experiments, because the calorimeter is particularly sensitive to the sample setup. As noted in the methods section (Section 2.4), these IC results were consistently reproduced over multiple experimental runs.

Similar trends in SI^{eff} values, aqueous Ca, sulfur, and Al concentrations, and solid phase assemblages are found in the gypsum containing aqueous cub- and orth-C_3A systems except for ½AH_3 (Fig. 4), which is undersaturated in the cub-C_3A system but is 'near-saturated' in the orth-C_3A system before complete gypsum dissolution. Significantly lower SI^{eff} values for ½AH_3 are also calculated in the sulfur-free cub-C_3A system compared to the corresponding orth-C_3A system (Fig. 1), which are related to the measured $Ca/Al_{[aq]}$ values, and result from the higher solubility of $Al_6O_{18}^{18-}$ ring structures in orth-C_3A relative to those in cub-C_3A in the respective aqueous solutions [45]. The relatively high, proportional and concurrent release of Na and Al measured in the orth-C_3A systems (Figs. 1A and 4A) supports this explanation because Na is intimately bound within the $Al_6O_{18}^{18-}$ ring

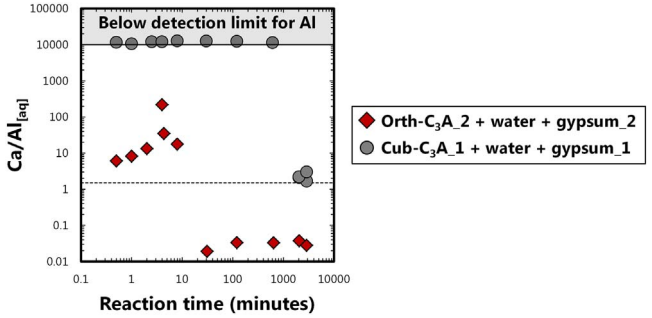

Fig. 6. $Ca/Al_{[aq]}$ values of supernatants collected from samples containing orth-C_3A_2 and gypsum_2 hydrated in water (red diamonds), and cub-C_3A_1 and gypsum_1 hydrated in water (grey circles). The dashed black horizontal line represents the molar Ca/Al ratio in bulk C_3A. (For interpretation of the references to colour in this figure legend, the reader is referred to the web version of this article.)

structures of this phase [65], i.e., dissolution of $Al_6O_{18}^{18-}$ rings in orth-C_3A releases both Na and Al into solution. The implications of cub-C_3A having relatively less soluble $Al_6O_{18}^{18-}$ ring structures than those present in orth-C_3A are now discussed.

3.3. Implications for fresh PC concrete

The results and analysis presented above points towards the bulk solution chemistry being the key rate controlling factor for orth-C_3A dissolution in water and in $CaSO_4$ containing aqueous solutions (Figs. 1A–C and 4A–C). The calculated SI^{eff} values for cub-C_3A in these systems (acting as a proxy for orth-C_3A) are similar in the presence and absence of gypsum, before complete gypsum consumption, which therefore does not point to crystal-chemical defects [66] controlling the orth-C_3A dissolution rate. Rather, the aqueous Al concentration is greatly reduced in the presence of gypsum relative to the sulfur-free orth-C_3A system, attributed mainly to the uptake of Al in ettringite, which would cause a greater driving force for orth-C_3A dissolution (of its $Al_6O_{18}^{18-}$ rings). Orth-C_3A dissolves faster than cub-C_3A in water in the presence of gypsum, which indicates that rheology and/or setting problems are likely in fresh PC concrete if too much orth-C_3A exists in PC without further modification of the solution chemistry, because fresh PC concrete typically contains calcium sulfate and a very low Al concentration [8,67] (these are the conditions needed for rapid orth-C_3A dissolution). Therefore, to avoid setting problems in PC concrete from rapid dissolution of orth-C_3A, the orth-C_3A content should be reduced and/or the solution chemistry should be modified (e.g., using admixtures) to increase its Al concentration.

Adsorption phenomena are, however, generally agreed to provide the key dissolution rate controlling factor(s) in cub-C_3A hydration [15,20,21,24,29,30,35,36]. The values of $Ca/Al_{[aq]} \gg 1.5$ as measured by ICP-OES in the cub-C_3A systems here are consistent with the presence of an Al-rich leached layer at the partially dissolved cub-C_3A/solution interface [30,45]. Recent research utilising solution (pH) and surface (zeta potential, Ca and sulfur *K*-edge XAS) chemical, and morphological (X-ray ptychography, scanning electron microscopy) methods suggests that this layer non-specifically adsorbs Ca and Ca-sulfur ion pair complexes and that the latter complexes in particular act to increase the local saturation extent near C_3A surface sites and inhibit dissolution [41]. The assignment of the Al-rich leached layer to a key role in this adsorption mechanism may explain why the dissolution of cub- and orth-C_3A are controlled by different factors, because this layer is less stable in systems containing orth-C_3A (higher alkali concentration) [45]. The specific complexation of Ca and SO_4^{2-} on cub-C_3A system was unsupported by the results obtained in that recent investigation, which is consistent with the geochemistry literature at pH > 12 [37–40,64].

If this hypothesis is true, i.e., that nonspecific adsorption of the Ca-sulfur ion pair complex is key to cub-C_3A dissolution inhibition, then this dissolution inhibiting effect should be reproduced in the presence

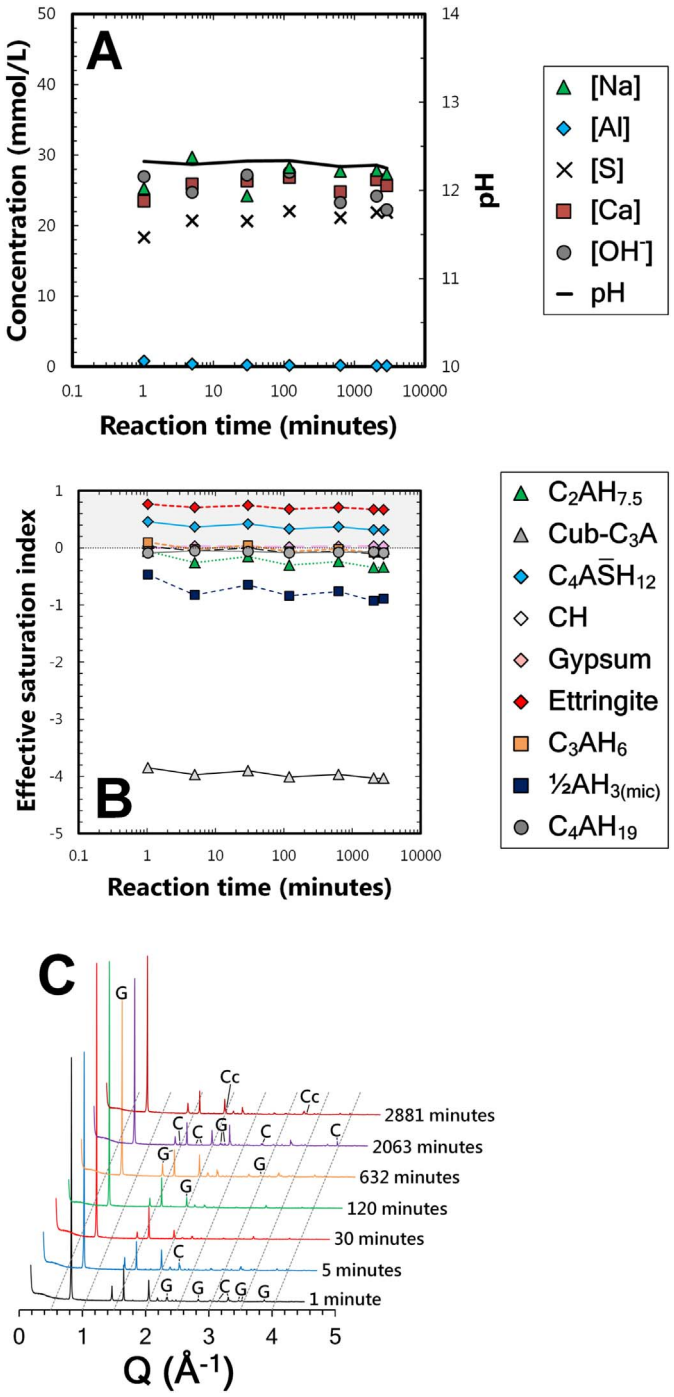

Fig. 7. Results from analysis of cub-C_3A_2 and gypsum_2 hydrated in a PNS solution at an equivalent bulk sulfur concentration to the PNS-free and gypsum containing cub-C_3A system (Fig. 4D–F). The phase identification labels in the diffractograms are C = cub-C_3A, G = gypsum and Cc = calcite. The grey and white regions in (B) and (E) represent supersaturation (SI^{eff} > 0) and undersaturation (SI^{eff} < 0) of the solid with respect to the aqueous phase, respectively. Microcrystalline is abbreviated as mic.

of Ca-Se ion pair complexes because the adsorption behaviour of SO_4^{2-} and SeO_4^{2-} are similar [68]. Further research, particularly in advancing understanding of the molecular structure of the cub-C_3A/solution interface [41], and experimental testing of cub-C_3A hydration in aqueous solutions similar to $CaSO_4$ [41], are needed to confirm this assignment.

That recent study [41] also showed that PNS adsorbs to the partially hydrated cub-C_3A surface at pH > 12. Figs. 7 and 8 show that PNS greatly retards cub-C_3A dissolution in the presence of gypsum relative to systems without PNS and at the same bulk sulfur concentration (Fig. 4D–F), consistent with that research. Ettringite and $C_4A\bar{S}H_{12}$ are supersaturated in this PNS containing system although the precipitation of these phases is effectively suppressed by the low dissolution extent of cub-C_3A (Fig. 7B–C). However, some cub-C_3A does dissolve here (Fig. 7A), with its Ca structures dissolving faster than its $Al_6O_{18}^{18-}$ ring structures ($Ca/Al_{[aq]} \gg 1.5$). The measured aqueous Al, Ca, sulfur, OH^-, and Na concentrations are similar up to 2881 min (~48 h) of hydration. Gypsum dissolution is also strongly retarded here, which is consistent with the saturated SI^{eff} values for this phase and/or may suggest that PNS has adsorbed onto this phase, inhibiting dissolution. A small amount of calcite ($C\bar{C}$, PDF# 00-05-0586) is observed to precipitate from superficial carbonation of the samples at 2881 min (~48 h) of hydration.

Complexation of PNS with the partially dissolved C_3A surface may be analogous to the mechanism by which cub-C_3A dissolution is inhibited by phosphate containing macromolecules, e.g., nitrile-tris(methylene) phosphonic acid ($N[CH_2PO(OH)_2]_3$) [69]. This compound adsorbs to the cub-C_3A surface and forms surface bound macromolecules that greatly retard dissolution. Therefore, the results presented here highlight the importance of the solution chemistry, e.g., the pH and aqueous Ca and sulfur concentrations, in addition to adsorption phenomena, on the rate controlling mechanisms of cub-C_3A hydration. In fresh PC systems the pH is generally > 12 [8,67,70,71] and so the surfaces of partially dissolved PC phases are predominantly deprotonated, which is a critically important consideration when investigating the behaviour of chemical admixtures and the solid/solution interface chemistry in C_3A and PC systems.

4. Conclusions

This paper has presented a solution chemistry focused analysis of orth- or cub-C_3A hydration in water, water with gypsum, as well as in a PNS containing aqueous solution in the presence of gypsum. In the sulfur-free systems, cub-C_3A was found to hydrate faster than orth-C_3A, with predominantly katoite precipitated. The $Ca/Al_{[aq]}$ values measured in the orth- and cub-C_3A samples were ≫1.5 and ≪1.5, respectively, which were attributed to a higher solubility of $Al_6O_{18}^{18-}$ ring structures in orth-C_3A than in cub-C_3A. This interpretation was supported by the direct relationship found between the dissolved Al and Na concentrations in the orth-C_3A samples. The relatively lower solubility of the $Al_6O_{18}^{18-}$ rings in cub-C_3A was proposed to play a key role in the formation of an Al-rich leached layer at the partially-dissolved cub-C_3A/solution interface, which itself influenced the dissolution rate controlling mechanism.

The XRD, ICP-OES, and thermodynamic modelling results indicated that the chemistries of the gypsum containing cub- and orth-C_3A samples were greatly modified once the gypsum source was completely consumed. Predominantly ettringite precipitated from solutions significantly supersaturated with respect to this phase before complete gypsum dissolution. Complete gypsum consumption occurred hours earlier in the orth-C_3A system, although effectively the same amount of heat was cumulatively released in both orth- and cub-C_3A systems by 48 h of hydration. On complete gypsum consumption, the dissolved Ca and sulfur concentrations decreased, the aqueous Al concentration increased, and ettringite was destabilised to $C_4A\bar{S}H_{12}$ and also to OH-AFm at later hydration times. The much lower Al concentration in the gypsum containing orth-C_3A system relative to the sulfur-free orth-C_3A system could explain the significantly increased dissolution rate of this phase in the former system. Therefore, the results suggest that orth-C_3A dissolution is controlled by the bulk solution chemistry in (gypsum containing) aqueous solutions.

The lower solubility of the $Al_6O_{18}^{18-}$ ring structures in cub-C_3A and the consequent formation of an Al-rich leached layer during dissolution was able to explain the key inhibiting action of adsorbed Ca-sulfur ion pair complexes on cub-C_3A dissolution. These findings were discussed

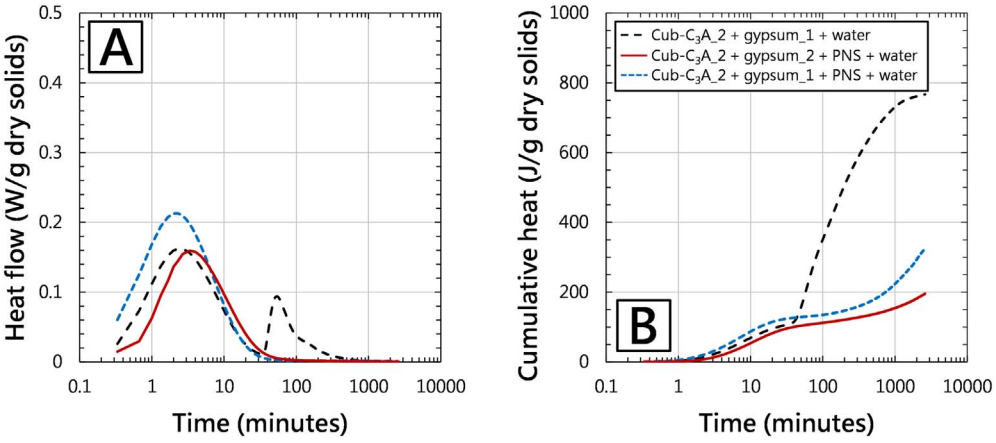

Fig. 8. (A) Heat flow and (B) cumulative heat released from cub-C_3A_2 and gypsum_1 hydrated in a PNS-containing aqueous solution (dashed blue lines), cub-C_3A_2 and gypsum_2 hydrated in a PNS-containing aqueous solution (solid red lines), and cub-C_3A_2 and gypsum_1 hydrated in water (dashed black lines and also shown in Fig. 5). (For interpretation of the references to colour in this figure legend, the reader is referred to the web version of this article.)

considering recently reported results, to more coherently describe the influence of adsorbed Ca and sulfur complexes on cub-C_3A hydration, in which the Ca-sulfur ion pair complex plays a key inhibiting role. However, additional experimental and modelling results are needed to confirm this conclusion.

Results obtained for cub-C_3A and gypsum hydrated in a PNS containing solution supported the dissolution inhibiting action of PNS being caused by adsorption, and that inclusion of PNS in the cub-C_3A-gypsum-water system greatly modifies the solution chemistry. No solid hydration products were identified by XRD in samples produced by reacting cub-C_3A and gypsum with the PNS-containing aqueous solution. Therefore, this paper demonstrates the importance of the solution chemistry, including adsorption effects, on cub- and orth-C_3A hydration in PC-relevant systems.

Supporting information

Additional particle size distribution, TGA and XRD results, and details of the XRF measurements for the solid precursors are provided in Appendix A; Appendix B contains additional TGA results for hydrated cub- and orth-C_3A samples after 4 min of hydration in water; and the thermodynamic database used in modelling calculations is shown in Appendix C.

Conflict of interest

The authors declare no competing financial interests.

Acknowledgements

The authors acknowledge the financial support from Siam Cement Public Company (SCG) Ltd, Thailand. E. D. Rodriguez and A. P. Kirchheim also acknowledge the financial support of CNPq BJT Grant number 406684/2013-8 and CNPq PQ Grant number 309949/2014-9. Priscila da Rosa acknowledges the financial support of Coordination for the Improvement of Higher Education Personnel (CAPES). The authors thank Timothy Teague for help with XRD and XRF, Andrew and Wenbo Yang for help with ICP-OES, the Lacer Team (Ceramic Laboratory – UFRGS) for the BET and particle size distribution measurements, Lucas S. Girotto for assistance with the IC measurements, and Jeff Higginbotham, Negassi Hadgu and Carlos Hernandez Cruz for help in the laboratory.

Appendix A. Supplementary data

Supplementary data to this article can be found online at http://dx.doi.org/10.1016/j.cemconres.2017.06.008.

References

[1] L.G. Baquerizo, T. Matschei, K.L. Scrivener, M. Saeidpour, L. Wadsö, Hydration states of AFm cement phases, Cem. Concr. Res. 73 (2015) 143–157.
[2] A.N. Christensen, T.R. Jensen, N.V.Y. Scarlett, I.C. Madsen, J.C. Hanson, Hydrolysis of pure and sodium substituted calcium aluminates and cement clinker components investigated by in situ synchrotron X-ray powder diffraction, J. Am. Ceram. Soc. 87 (2004) 1488–1493.
[3] L. Black, C. Breen, J. Yarwood, C.S. Deng, J. Phipps, G. Maitland, Hydration of tricalcium aluminate (C_3A) in the presence and absence of gypsum-studied by Raman spectroscopy and X-ray diffraction, J. Mater. Chem. 16 (2006) 1263–1272.
[4] A.C. Jupe, X. Turrillas, P. Barnes, S.L. Colston, C. Hall, D. Häusermann, M. Hanfland, Fast in situ X-ray-diffraction studies of chemical reactions: a synchrotron view of the hydration of tricalcium aluminate, Phys. Rev. B 53 (1996) R14697–R14700.
[5] H.F.W. Taylor, Cement Chemistry, 2nd ed, Thomas Telford Publishing, London, 1997.
[6] H.W.W. Pollitt, A.W. Brown, The Distribution of Alkalis in Portland Cement Clinker, Proceedings of the Proceedings of the 5th International Symposium on the Chemistry of Cement, Tokyo, 1968.
[7] D. Jansen, C. Stabler, F. Goetz-Neunhoeffer, S. Dittrich, J. Neubauer, Does ordinary Portland cement contain amorphous phase? A quantitative study using an external standard method, Powder Diffract. 26 (2011) 31–38.
[8] B. Lothenbach, F. Winnefeld, Thermodynamic modelling of the hydration of Portland cement, Cem. Concr. Res. 36 (2006) 209–226.
[9] G.A.C.M. Spierings, H.N. Stein, The influence of Na_2O on the hydration of C_3A. I. Paste hydration, Cem. Concr. Res. 6 (1976) 265–272.
[10] F.C. Lee, H.M. Banda, F.P. Glasser, Substitution of Na, Fe and Si in tricalcium aluminate and the polymorphism of solid solutions, Cem. Concr. Res. 12 (1982) 237–246.
[11] M. Regourd, A. Guinier, The Crystal Chemistry of the Constituents of Portland Cement Clinker, Proceedings of the Proceedings of the 6th International Congress on the Chemistry of Cement, Moscow, 1974.
[12] I. Maki, Nature of the prismatic dark interstitial material in Portland cement clinker, Cem. Concr. Res. 3 (1973) 295–313.
[13] L. Gobbo, L.L. Sant'Agostino, L. Garcez, C_3A polymorphs related to industrial clinker alkalies content, Cem. Concr. Res. 34 (2004) 657–664.
[14] C. Ostrowski, J. Żelazny, Solid solutions of calcium aluminates C_3A, $C_{12}A_7$ and CA with sodium oxide, J. Therm. Anal. Calorim. 75 (2004) 867–885.
[15] H. Minard, S. Garrault, L. Regnaud, A. Nonat, Mechanisms and parameters controlling the tricalcium aluminate reactivity in the presence of gypsum, Cem. Concr. Res. 37 (2007) 1418–1426.
[16] A. Quennoz, K.L. Scrivener, Hydration of C_3A–gypsum systems, Cem. Concr. Res. 42 (2012) 1032–1041.
[17] A.P. Kirchheim, D.C. Dal Molin, P. Fischer, A.-H. Emwas, J.L. Provis, P.J.M. Monteiro, Real-time high-resolution X-ray imaging and nuclear magnetic resonance study of the hydration of pure and Na-doped C_3A in the presence of sulfates, Inorg. Chem. 50 (2011) 1203–1212.
[18] A.P. Kirchheim, V. Fernàndez-Altable, P.J.M. Monteiro, D.C.C. Dal Molin, I. Casanova, Analysis of cubic and orthorhombic C_3A hydration in presence of gypsum and lime, J. Mater. Sci. 44 (2009) 2038–2045.
[19] D. Stephan, S. Wistuba, Crystal structure refinement and hydration behaviour of doped tricalcium aluminate, Cem. Concr. Res. 36 (2006) 2011–2020.
[20] M.M. Alonso, F. Puertas, Adsorption of PCE and PNS superplasticisers on cubic and orthorhombic C_3A. Effect of sulfate, Constr. Build. Mater. 78 (2015) 324–332.
[21] S. Pourchet, L. Regnaud, J.P. Perez, A. Nonat, Early C_3A hydration in the presence of different kinds of calcium sulfate, Cem. Concr. Res. 39 (2009) 989–996.
[22] D.A. Silva, P.J.M. Monteiro, Early formation of ettringite in tricalcium aluminate–calcium hydroxide–gypsum dispersions, J. Am. Ceram. Soc. 90 (2007) 614–617.
[23] K.L. Scrivener, Backscattered electron imaging of cementitious microstructures: understanding and quantification, Cem. Concr. Compos. 26 (2004) 935–945.
[24] K.L. Scrivener, A. Nonat, Hydration of cementitious materials, present and future, Cem. Concr. Res. 41 (2011) 651–665.

[25] D. Jansen, F. Goetz-Neunhoeffer, B. Lothenbach, J. Neubauer, The early hydration of ordinary Portland cement (OPC): an approach comparing measured heat flow with calculated heat flow from QXRD, Cem. Concr. Res. 42 (2012) 134–138.

[26] P.W. Brown, L.O. Liberman, G. Frohnsdorff, Kinetics of the early hydration of tricalcium aluminate in solutions containing calcium sulfate, J. Am. Ceram. Soc. 67 (1984) 793–795.

[27] P.K. Mehta, Effect of lime on hydration of pastes containing gypsum and calcium aluminates or calcium sulfoaluminate, J. Am. Ceram. Soc. 56 (1973) 315–319.

[28] S. Chatterji, J.W. Jeffery, Studies of early stages of paste hydration of cement compounds, II, J. Am. Ceram. Soc. 46 (1963) 187–191.

[29] R.F. Feldman, V.S. Ramachandran, The influence of $CaSO_4.2H_2O$ upon the hydration character of $3CaO.Al_2O_3$, Mag. Concr. Res. 66 (1966) 185–196.

[30] J.A.N. Skalny, M.E. Tadros, Retardation of tricalcium aluminate hydration by sulfates, J. Am. Ceram. Soc. 60 (1977) 174–175.

[31] M. Collepardi, G. Baldini, M. Pauri, M. Corradi, Tricalcium aluminate hydration in the presence of lime, gypsum or sodium sulfate, Cem. Concr. Res. 8 (1978) 571–580.

[32] A.U.D. Traetteberg, P.E. Grattan-Bellew, Hydration of $3CaO{\cdot}Al_2O_3$ and $3CaO{\cdot}Al_2O_3$ + gypsum with and without $CaCl_2$, J. Am. Ceram. Soc. 58 (1975) 221–227.

[33] M.E. Tadros, W.Y. Jackson, J.A.N. Skalny, Study of the dissolution and electrokinetic behavior of tricalcium aluminate, in: M. Kerker (Ed.), Hydrosols and Rheology, Academic Press, London, 1976, pp. 211–223.

[34] P.W. Brown, Kinetics of tricalcium aluminate and tetracalcium aluminoferrite hydration in the presence of calcium sulfate, J. Am. Ceram. Soc. 76 (1993) 2971–2976.

[35] K.L. Scrivener, P. Juilland, P.J.M. Monteiro, Advances in understanding hydration of Portland cement, Cem. Concr. Res. 78A (2015) 38–56.

[36] J.W. Bullard, H.M. Jennings, R.A. Livingston, A. Nonat, G.W. Scherer, J.S. Schweitzer, K.L. Scrivener, J.J. Thomas, Mechanisms of cement hydration, Cem. Concr. Res. 41 (2011) 1208–1223.

[37] H. Wijnja, C.P. Schulthess, Vibrational spectroscopy study of selenate and sulfate adsorption mechanisms on Fe and Al (hydr)oxide surfaces, J. Colloid Interf. Sci. 229 (2000) 286–297.

[38] L. Sigg, W. Stumm, The interaction of anions and weak acids with the hydrous goethite (α-FeOOH) surface, Colloid Surf. 2 (1981) 101–117.

[39] L. Charlet, N. Dise, W. Stumm, Acidification of soil sulfate adsorption on a variable charge soil and on reference minerals, Agric. Ecosyst. Environ. 47 (1993) 87–102.

[40] D. Peak, Adsorption mechanisms of selenium oxyanions at the aluminum oxide/water interface, J. Colloid Interf. Sci. 303 (2006) 337–345.

[41] R.J. Myers, G. Geng, J. Li, E.D. Rodríguez, J. Ha, P. Kidkhunthod, G. Sposito, L.N. Lammers, A.P. Kirchheim, P.J.M. Monteiro, Role of adsorption phenomena in cubic tricalcium aluminate dissolution, Langmuir 33 (2017) 45–55.

[42] D. Bonen, S.L. Sarkar, The superplasticizer adsorption capacity of cement pastes, pore solution composition, and parameters affecting flow loss, Cem. Concr. Res. 25 (1995) 1423–1434.

[43] H. Uchikawa, S. Hanehara, D. Sawaki, The role of steric repulsive force in the dispersion of cement particles in fresh paste prepared with organic admixture, Cem. Concr. Res. 27 (1997) 37–50.

[44] D. Marchon, R.J. Flatt, Impact of chemical admixtures on cement hydration, in: P.-C. Aïtcin, R.J. Flatt (Eds.), Science and Technology of Concrete Admixtures, Elsevier, Cambridge, 2016.

[45] F.P. Glasser, M.B. Marinho, Early stages of the hydration of calcium aluminate and its sodium-containing solid solutions, Br. Ceram. Soc. J. 35 (1984) 222–236.

[46] G. Geng, R.J. Myers, A.L.D. Kilcoyne, J. Ha, P.J.M. Monteiro, Ca $L_{2,3}$-edge near edge X-ray absorption fine structure of tricalcium aluminate, gypsum, and calcium (sulfo)aluminate hydrates, Am. Mineral. 102 (2017) 900.

[47] D.A. Kulik, T. Wagner, S.V. Dmytrieva, G. Kosakowski, F.F. Hingerl, K.V. Chudnenko, U. Berner, GEM-Selektor geochemical modeling package: revised algorithm and GEMS3K numerical kernel for coupled simulation codes, Comput. Geosci. 17 (2013) 1–24.

[48] T. Wagner, D.A. Kulik, F.F. Hingerl, S.V. Dmytrieva, GEM-Selektor geochemical modeling package: TSolMod library and data interface for multicomponent phase models, Can. Mineral. 50 (2012) 1173–1195.

[49] H.C. Helgeson, D.H. Kirkham, G.C. Flowers, Theoretical prediction of the thermodynamic behavior of aqueous electrolytes at high pressures and temperatures: IV. Calculation of activity coefficients, osmotic coefficients, and apparent molal and standard and relative partial molal properties to 600°C and 5 kb, Am. J. Sci. 281 (1981) 1249–1516.

[50] B. Lothenbach, T. Matschei, G. Möschner, F.P. Glasser, Thermodynamic modelling of the effect of temperature on the hydration and porosity of Portland cement, Cem. Concr. Res. 38 (2008) 1–18.

[51] T. Matschei, B. Lothenbach, F.P. Glasser, Thermodynamic properties of Portland cement hydrates in the system $CaO\text{-}Al_2O_3\text{-}SiO_2\text{-}CaSO_4\text{-}CaCO_3\text{-}H_2O$, Cem. Concr. Res. 37 (2007) 1379–1410.

[52] G. Möschner, B. Lothenbach, J. Rose, A. Ulrich, R. Figi, R. Kretzschmar, Solubility of Fe–ettringite ($Ca_6[Fe(OH)_6]_2(SO_4)_3{\cdot}26H_2O$), Geochim. Cosmochim. Acta 72 (2008) 1–18.

[53] W. Hummel, U. Berner, E. Curti, F.J. Pearson, T. Thoenen, Nagra/PSI Chemical Thermodynamic Database 01/01, Universal Publishers, Parkland, Florida, 2002.

[54] T. Thoenen, D.A. Kulik, Nagra/PSI Chemical Thermodynamic Database 01/01 for the GEM-Selektor (V.2-PSI) Geochemical Modeling Code, Paul Scherrer Institute, Villigen, (2003).

[55] T. Thoenen, W. Hummel, U. Berner, The PSI/Nagra chemical thermodynamic database 12/07: present status and future developments, Mineral. Mag. 77 (2013) 2327.

[56] G. Möschner, B. Lothenbach, F. Winnefeld, A. Ulrich, R. Figi, R. Kretzschmar, Solid solution between Al-ettringite and Fe-ettringite ($Ca_6[Al_{1-x}Fe_x(OH)_6]_2(SO_4)_3{\cdot}26H_2O$), Cem. Concr. Res. 39 (2009) 482–489.

[57] B. Lothenbach, L. Pelletier-Chaignat, F. Winnefeld, Stability in the system $CaO–Al_2O_3–H_2O$, Cem. Concr. Res. 42 (2012) 1621–1634.

[58] M. Balonis, F.P. Glasser, The density of cement phases, Cem. Concr. Res. 39 (2009) 733–739.

[59] R.A. Robie, B.S. Hemingway, Thermodynamic Properties of Minerals and Related Substances at 298.15 K and 1 bar (10^5 Pascals) Pressure and at Higher Temperatures, United States Government Printing Office, Washington D.C., 1995.

[60] H.C. Helgeson, J.M. Delany, H.W. Nesbitt, Summary and critique of the thermodynamic properties of rock-forming minerals, Am. J. Sci. 278-A (1978) 1–229.

[61] D. Garvin, V.B. Parker, H.J. White Jr., CODATA Thermodynamic Tables Selections for Some Compounds of Calcium and Related Mixtures: A Prototype set of Tables, Hemisphere Pub. Corp, Washington, 1987.

[62] A.I. Boikova, A.I. Domansky, V.A. Paramonova, G.P. Stavitskaja, V.M. Nikushchenko, The influence of Na_2O on the structure and properties of $3CaO{\cdot}Al_2O_3$, Cem. Concr. Res. 7 (1977) 483–492.

[63] K. Maher, N.C. Johnson, A. Jackson, L.N. Lammers, A.B. Torchinsky, K.L. Weaver, D.K. Bird, G.E. Brown, A spatially resolved surface kinetic model for forsterite dissolution, Geochim. Cosmochim. Acta 174 (2016) 313–334.

[64] I. Siretanu, D. Ebeling, M.P. Andersson, S.L.S. Stipp, A. Philipse, M.C. Stuart, D. van den Ende, F. Mugele, Direct observation of ionic structure at solid-liquid interfaces: a deep look into the stern layer, Sci. Rep. 4 (2014) 4956.

[65] F. Nishi, Y. Takéuchi, The Al_6O_{18} rings of tetrahedra in the structure of $Ca_{8.5}NaAl_6O_{18}$, Acta Cryst. B31 (1975) 1169–1173.

[66] A.C. Lasaga, A. Lüttge, Mineralogical approaches to fundamental crystal dissolution kinetics, Am. Mineral. 89 (2004) 527–540.

[67] D. Rothstein, J.J. Thomas, B.J. Christensen, H.M. Jennings, Solubility behavior of Ca-, S-, Al-, and Si-bearing solid phases in Portland cement pore solutions as a function of hydration time, Cem. Concr. Res. 32 (2002) 1663–1671.

[68] G. Sposito, The Chemistry of Soils, 2nd ed., Oxford University Press, New York, 2008.

[69] M. Bishop, S.G. Bott, A.R. Barron, A new mechanism for cement hydration inhibition: solid-state chemistry of calcium nitrilotris(methylene)triphosphonate, Chem. Mater. 15 (2003) 3074–3088.

[70] B. Lothenbach, D. Rentsch, E. Wieland, Hydration of a silica fume blended low-alkali shotcrete cement, Phys. Chem. Earth 70–71 (2014) 3–16.

[71] J.L. García Calvo, A. Hidalgo, C. Alonso, L. Fernández Luco, Development of low-pH cementitious materials for HLRW repositories: resistance against ground waters aggression, Cem. Concr. Res. 40 (2010) 1290–1297.